European Spine Journal (2022) 31:2383–2398
https://doi.org/10.1007/s00586-022-07292-x

ORIGINAL ARTICLE

Dysfunctional paraspinal muscles in adult spinal deformity patients lead to increased spinal loading

Masoud Malakoutian[1,2] · Alex M. Noonan[3] · Iraj Dehghan-Hamani[1,2] · Shun Yamamoto[2,4] · Sidney Fels[5] · David Wilson[6] · Majid Doroudi[7] · Peter Schutz[8] · Stephen Lewis[9] · Tamir Ailon[2,6] · John Street[2,6] · Stephen H. M. Brown[3] · Thomas R. Oxland[1,2,6]

Received: 15 October 2021 / Revised: 17 May 2022 / Accepted: 6 June 2022 / Published online: 16 July 2022

Abstract

Purpose Decreased spinal extensor muscle strength in adult spinal deformity (ASD) patients is well-known but poorly understood; thus, this study aimed to investigate the biomechanical and histopathological properties of paraspinal muscles from ASD patients and predict the effect of altered biomechanical properties on spine loading.

Methods 68 muscle biopsies were collected from nine ASD patients at L4–L5 (bilateral multifidus and longissimus sampled). The biopsies were tested for muscle fiber and fiber bundle biomechanical properties and histopathology. The small sample size (due to COVID-19) precluded formal statistical analysis, but the properties were compared to literature data. Changes in spinal loading due to the measured properties were predicted by a lumbar spine musculoskeletal model.

Results Single fiber passive elastic moduli were similar to literature values, but in contrast, the fiber bundle moduli exhibited a wide range beyond literature values, with 22% of 171 fiber bundles exhibiting very high elastic moduli, up to 20 times greater. Active contractile specific force was consistently less than literature, with notably 24% of samples exhibiting no contractile ability. Histological analysis of 28 biopsies revealed frequent fibro-fatty replacement with a range of muscle fiber abnormalities. Biomechanical modelling predicted that high muscle stiffness could increase the compressive loads in the spine by over 500%, particularly in flexed postures.

Discussion The histopathological observations suggest diverse mechanisms of potential functional impairment. The large variations observed in muscle biomechanical properties can have a dramatic influence on spinal forces. These early findings highlight the potential key role of the paraspinal muscle in ASD.

Keywords Adult spinal deformity · Biomechanics · Biochemical · Muscle · Sarcomere · Passive stiffness

Introduction

Aging of the spine results in a sagittal alignment disorder, typically characterized by loss of lumbar lordosis and thoracic hyperkyphosis, in 20–40% of the adult population, with a recent report suggesting that up to 2/3 of individuals over 65 years old suffer from some spinal deformity [1, 2]. Approximately 80% of these individuals are female [3]. While various risk factors such as vertebral fractures, neurological dysfunction, postural and degenerative

✉ Thomas R. Oxland
toxland@mail.ubc.ca

1 Department of Mechanical Engineering, University of British Columbia, Vancouver, BC, Canada

2 ICORD, Blusson Spinal Cord Centre, 3rd Floor, 818 West 10th Avenue, Vancouver, BC V5Z 1M9, Canada

3 Department of Human Health and Nutritional Sciences, University of Guelph, Guelph, ON, Canada

4 Department of Orthopaedic Surgery, Jikei University Graduate School of Medicine, Tokyo, Japan

5 Department of Electrical and Computer Engineering, University of British Columbia, Vancouver, BC, Canada

6 Department of Orthopaedics, University of British Columbia, Vancouver, BC, Canada

7 Department of Cellular and Physiological Sciences, University of British Columbia, Vancouver, BC, Canada

8 Department of Pathology and Laboratory Medicine, University of British Columbia, Vancouver, BC, Canada

9 Department of Surgery, University of Toronto, Toronto, ON, Canada

intervertebral disc changes, and genetic predisposition partly explain sagittal balance disorder [1, 4], a critical causative factor in adult spinal deformity (ASD) appears to be paraspinal and spinopelvic muscular dysfunction [5–10]. This is particularly true in the case of post-surgical kyphotic deformities such as junctional kyphosis.

The standard of care for ASD patients who suffer from significant pain and functional loss is multi-level spinal decompression, realignment, and fusion [11]. While most patients benefit from these complex surgeries, up to 50% will develop some abnormal changes at the vertebral level proximal to the spinal instrumentation [12]. In severe cases, termed Proximal Junctional Failure (PJF), re-operation is required, which entails additional risk and morbidity for patients and considerable cost to the health care system.

There are a number of risk factors for PJF that have been identified from clinical studies. These include geometric features of the spine and pelvis (e.g. magnitude of thoracic kyphosis), surgical factors (e.g. location of uppermost instrumented vertebra), and other risk factors (e.g. age more than 55 years old, low bone density). A clinical scoring scheme to predict PJF that incorporates these risk factors was introduced in 2020 [3]. Notably, this scoring system is based on clinical observation rather than a mechanistic understanding of the problem. Although a low volume of posterior musculature has recently been identified as an independent risk factor for the development of PJF [13], this factor is currently not included in the clinical estimation of PJF risk.

Reduced lumbar and thoracic extensor muscle strength may arise from small muscle anatomical cross-sectional areas, low levels of activation, or short muscle moment arms, all of which have been observed to some extent in ASD patients compared to the normal population [14–16]. However, there are other muscle biomechanical properties that contribute to force production capacity, which include the passive elastic modulus, slack sarcomere length (beyond which passive force starts to develop), in-situ sarcomere length (i.e. posture-dependent sarcomere lengths, which influence both passive and active force generating capabilities), and specific force (maximal active contractile force divided by cross-sectional area). These muscle properties are known to vary in the lower and upper extremity with different diseases [17–21], and changes in these properties can have profound biomechanical implications.

Comparatively little is known about the changes of paraspinal muscle with injury and disease. The passive elastic modulus of posterior paraspinal muscles has been measured in only one human study of a mixed group of degenerative spine patients [22]. They found multifidus to be 1.5 times stiffer than erector spinae and slack sarcomere lengths at the fiber bundle level to vary between multifidus, longissimus, and iliocostalis [22]. In animal studies, passive elastic modulus of paraspinal muscles has been shown to increase after a disc injury in rabbits [16], or after spinal surgery in rats [23]. Noonan et al. [24] demonstrated a decrease in paraspinal muscle specific force in ENT1 KO mice (calcified spines) compared to wild type mice, suggesting the intrinsic force generating capability of the paraspinal muscles may become compromised with spinal pathology. These observations suggest that paraspinal muscles are considerably adaptive similar to muscles of the extremities.

Given the clear importance of paraspinal muscle for proper functioning of the spine and the observations of muscle weakness in ASD patients, our primary objective was to characterize the biomechanical properties and histopathological features of the multifidus and longissimus muscles in ASD patients. Our secondary objective was to predict the effect of changes in these biomechanical properties on spine loading using a musculoskeletal model.

Materials and methods

This study was approved by the University of British Columbia Clinical Research Ethics Board (UBC CREB) and Vancouver Coastal Health Research Institute (VCHRI), Vancouver, Canada. All recruited patients were informed of the study and signed the consent forms.

Patient demographics and study design

Patients enrolled in this study were recruited from a spine surgery practice and they were all candidates for surgery. Note that the relationship between the degree of degenerative changes in the spinal vertebrae, discs and facet joints, and the condition of the posterior spinal musculature is as yet poorly understood. In clinical practice, there is an almost unlimited variability in the location, nature, degree, structural consequence and resultant symptoms of the degenerative changes seen in adult spinal deformity. The heterogenous and equally inconsistent nature of these changes make correlation with muscle property findings and with clinical presentation and treatment outcome very challenging. In order to mitigate this heterogeneity, and to provide reliable, broad subgroups that would allow meaningful analysis, we chose to examine the three common categories of clinical presentation of adult spinal deformity: I) patients with multilevel degenerative lumbar disease with no sagittal imbalance (sagittal vertical alignment (SVA) < 5 cm) and with no radiographic compensatory mechanisms recruited; II) patients with multilevel degenerative lumbar disease with no sagittal imbalance, maintained through effective recruitment

of compensatory mechanisms (i.e. muscle mediated compensatory mechanisms such as pelvic retroversion, segmental hyperlordosis, segmental retrolisthesis and thoracic hypokyphosis were sufficient to maintain a normal sagittal vertical alignment, i.e. SVA < 5 cm); and III) patients with multilevel degenerative lumbar disease with positive sagittal imbalance despite recruitment of multiple compensatory mechanisms (i.e. the aforementioned muscle mediated compensatory mechanisms were insufficient, resulting in abnormal SVA > 5 cm). This patient categorization is based on both reliable radiographic parameters and validated clinical correlates, and we believe it allows meaningful and clinically impactful conclusions to be drawn from our translational work.

A power analysis suggested that 14 patients were required for detecting a 30% difference in passive elastic modulus (i.e. primary outcome) of the multifidus and longissimus (e.g. 60 kPa vs. 80 kPa) based on data presented by Ward et al. [22]. A smaller number of patients was sufficient for a similar analysis of in-situ sarcomere length, but 14 patients per group were targeted.

In total, nine patients were recruited between September 2019 and March 2020 before the study was halted by the COVID-19 pandemic; four belonged to group I, three to group II, and two to group III. The demographics of the patients are presented in Table 1. Due to the small sample sizes, no statistical analysis was performed, but we did compare our data to literature values for human degenerative spine patients [22, 25] and age-matched lower limb muscle (vastus lateralis) [26–29].

Two types of biopsies were required and obtained during standard open spine surgery. Type A biopsies used a special biopsy clamp for measurement of in-situ sarcomere length, while Type B biopsies were obtained through a blunt cut and were divided into two halves: one half (Type B1) was used for active and passive biomechanical testing, while the other half (Type B2) was snap frozen for histopathological analysis. Overall, four Type A, four Type B1, and four Type B2 biopsies were collected from each patient, all at L4–L5, from left longissimus, left multifidus, right multifidus, and right longissimus (Fig. 1). Facet joints were used as landmarks, medial to which multifidus and lateral to which longissimus were accessed through a posterior midline incision.

Biopsy acquisition and testing

Biopsy type A—in-situ sarcomere length

Inside the operating room, immediately after the biopsies were collected, the clamps were transferred into Type-A-Samples container filled with formaldehyde (see Appendix B4 and 5 of [30] for more detail on biopsy acquisition). After fixation for a minimum of 48 hours, the biopsies were removed from the clamps and dissected under a stereomicroscope (Nikon, 0.63 X, Japan) to separate muscle fiber bundles. Using a diode laser (S1FC660, Thorlabs, Newton, NJ, USA; wavelength = 660 nm; beam diameter = 0.8 mm) each fiber bundle was transilluminated and the resulting diffraction pattern was used to calculate the in-situ sarcomere

Table 1 Demographics of the patients categorized into three groups: I) had multilevel degenerative lumbar disease with no sagittal imbalance (SVA < 5 cm) and no compensatory mechanisms recruited; II) had multilevel degenerative lumbar disease with no sagittal imbalance (SVA < 5 cm), maintained through effective recruitment of compensatory mechanisms; and III) had multilevel degenerative lumbar disease with positive sagittal imbalance (SVA > 5 cm) despite recruitment of multiple compensatory mechanisms

Ptnt #	Sex	Age (yrs)	Diagnosis	Coronal deformity			Group
				Levels affected	Severity (cobb angle)	Apex (two-ends)	
1	F	70	Scoliosis, degenerative, Second, acquired	T10–L4	Severe (58°)	L1 (T11–L3)	III
2	M	64	Spinal stenosis	L4–S1	Moderate (30°)	L2 (L1–L3)	II
3	M	61	Spinal stenosis	L4–L5	Very Mild (8°)	L2 (T12–L4)	I
4	M	75	Spondylosis	L2–S1	Mild (17°)	L2 (L2–L4)	III
5	M	71	Spinal stenosis	L2–L4	Mild (13°)	T12–L1 (T10–L2)	I
6	F	59	Spinal stenosis	L5–S1	Mild (16°)	L3 (L2–L4)	I
7	F	70	Spinal stenosis	L2–S1	Very Mild (4°)	L2 (T12–L4)	II
8	M	73	Spinal stenosis	L3–L5	None (0°)	None	I
9	F	51	Scoliosis, degenerative, Second, acquired	T9–S2 &ILIUM	Severe (57°)	L2 (T12–L3)	II

All patients recruited for this study were operated at Vancouver General Hospital

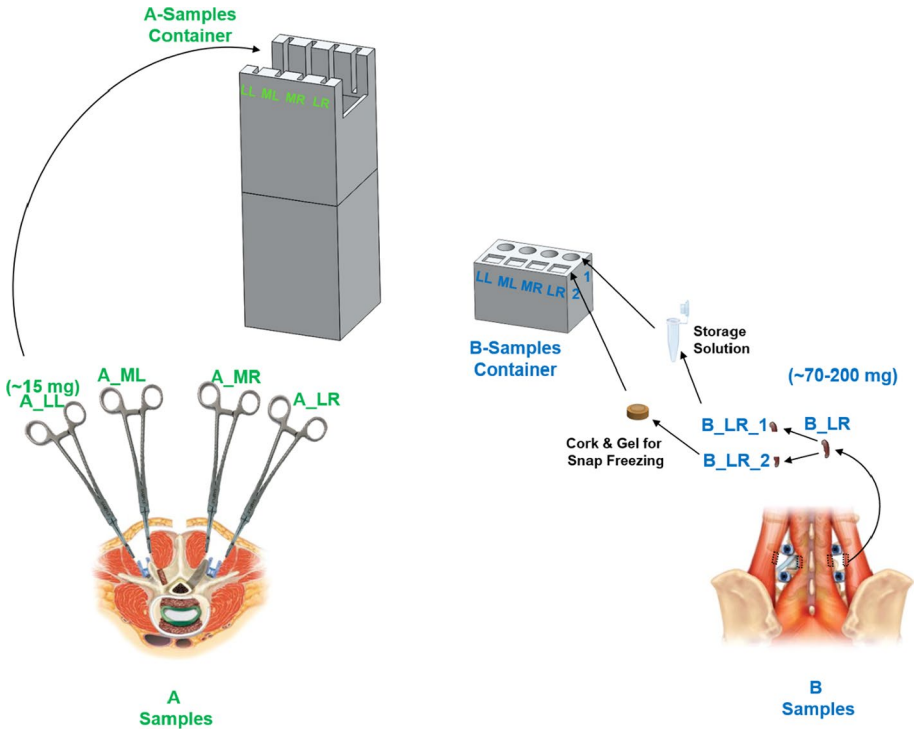

Fig. 1 Biopsies collected from each patient. Type A biopsies needed a special biopsy clamp for measurement of in-situ sarcomere length, while Type B biopsies were obtained through a blunt cut and were divided into two halves: one half (Type B1) was used for biomechanical testing, while the other half (Type B2) was snap frozen for histopathological analysis. Overall, four Type A, four Type B1, and four Type B2 biopsies were collected from each patient, all at L4–L5, and from left longissimus (LL), left multifidus (ML), right multifidus (MR), and right longissimus (LR). The anatomical artwork is adapted from [42] with permission from the JNS publishing group and is copyright protected. Permission for any re-use must be secured through JNS publishing group

length. From each biopsy, three fiber bundles were tested and the average was considered as the in-situ sarcomere length.

Biopsy type B1—passive elastic modulus, slack sarcomere length, and specific force

One half of Type B biopsies (Type B1) were placed inside falcon tubes filled with a dissecting solution [24]. The tubes were immediately placed inside an ice container at 0 °C and within two hours were transferred to the lab. Type B1 biopsies were further divided into smaller pieces/bundles: half of the pieces were transferred into a storage solution, kept at 4 °C for 24 hours, and then preserved at − 20 °C until they were tested for passive properties within two weeks [31]. The remaining pieces were further permeabilized by Brij 58 solution, transferred to a storage solution, and kept at – 80 °C until they were tested for active contractile specific force (see [24] for more details).

To assess slack sarcomere lengths and passive elastic modulus, a minimum of three fibers and six fiber bundles (14 ± 7 fibers ensheathed in their extracellular matrix) were extracted from each biopsy [31]. Each fiber/fiber bundle was mounted and tied onto two pins, one pin attached to a force transducer (400A, Aurora Scientific, Aurora, Ontario, Canada) and the other pin to a length controller (CRK523PMAP, Oriental Motor, Torrance, CA, USA). The fibers/fiber bundles were stretched until reaching the slack length, where passive force was first detected. At this point, the slack sarcomere length was measured with a resolution of ~ 10 nm from the diffraction pattern generated when transilluminating the fibers/fiber bundles using a diode laser. Also, top-view and side-view diameters of the fiber/fiber bundle were measured at three points across the fiber/fiber bundle using a stereo microscope (SteREO Discovery. V8, Zeiss, Plan-Apochromat 0.63x). Each fiber/fiber bundle was then stretched by 4 to 8 increments, each applying 10% strain at a rate of 10% strain per second, followed by four minutes relaxation. The sarcomere lengths and force at the end of each increment were used to calculate the engineering strains and stresses, respectively. A tangent to the strain–stress curve at 30% strain was used to represent the passive elastic modulus of the fiber/fiber bundle.

Single fiber specific force was measured at 15 °C, in solutions described elsewhere [24]. Briefly, single fibers were secured with monofilament sutures to pins on either side, one to a force transducer (Aurora Scientific, model 403A) and the other to servomotor lever arm (Aurora Scientific, model 322C). The fiber length was adjusted to obtain a sarcomere length of 2.7 μm using a high-speed camera (HVSL, Aurora Scientific 901B). Fiber length (Lo) was measured by aligning the innermost portion of the sutures at each end of the fiber with the crosshairs of a microscope eyepiece graticule. Fiber diameter was measured at 3 locations along the fiber length; from these measurements fiber cross-sectional area (CSA) was calculated (assuming a cylindrical shape). Relaxed single fibers were maximally activated by immersion in a chamber containing

a high-Ca2 + activating solution (pCa 4.2). Force and length data were sampled at 10,000 Hz. Maximal force was calculated as the peak force achieved in activating solution minus the resting force in relaxing solution, which was then divided by the fiber CSA to give a measure of specific force. After completion of this test the fiber was placed in 15 µl of solubilization buffer and stored at − 80 °C for a minimum of 48 hours. The myosin heavy chain (MHC) composition of the fiber (i.e. fiber type) was determined by sodium dodecyl sulfate–polyacrylamide gel electrophoresis (SDS–PAGE) as in [24].

Biopsy type B2—histopathology

For histopathology analysis, the other halves of Type B biopsies (Type B2) were transferred fresh in a moist environment to the lab and were snap frozen by placing them on a cork covered with Tragacanth gel and dropping them into isopentane cooled by liquid nitrogen. The samples were stored at − 80 °C until they were sectioned at 10 µm thickness.

Sections were stained with hematoxylin and eosin (HE) and gomori trichrome (GT) for morphology, nicotinamide adenine dinucleotide hydrogen tetrazonium reductase (NADH) to assess internal structure, and combined succinic dehydrogenase and cytochromec oxidase (COX/SDH) for mitochondrial enzymes. Immunohistochemical staining was performed for fast, slow, and neonatal myosin to assess fiber type and regeneration. The magnitude and main types of abnormalities were identified for all biopsies. Sections were analyzed by an experienced myo-pathologist (PS) blinded to patient demographics.

Musculoskeletal modeling

To explore the influence of measured biomechanical properties on spinal loading, an enhanced validated musculoskeletal model of the lumbar spine with 210 muscles was employed [32]. Briefly, the model consisted of the sacrum and pelvis (both fixed to the ground), five mobile lumbar vertebrae connected through 6-DOF springs (representing the stiffness of each pair of adjacent vertebrae with their connecting ligaments, facet joints, and intervertebral disc along three translational and three rotational degrees of freedom); and the thoracic spine that was rigidly fixed to the L1. Muscles were modeled as Hill-type musculotendon actuators, whose active and passive forces were determined using the force–length and force–velocity curves parametrized by Millard et al. [33] (see [32] for further details on muscle properties and calculation of its forces).

For two static postures (standing and 36° lumbar spine flexion), the intradiscal pressure (IDP) at L4–L5 was contrasted between three different models: one model with no muscle degeneration (baseline model) and two other models in which 25% (representing mild degeneration) and 75% (representing severe degeneration) of the contractile tissue was replaced by degenerated (stiffer) muscle fiber bundles in each of multifidus, longissimus, and iliocostalis (Fig. 2). Based on the rule of mixtures (see Appendix 1), the targeted muscles were estimated to be 1.44 and 2.32 times stiffer (than baseline) in the mild and severe degeneration models, respectively. In addition, maximum contractile force (i.e. specific force) of the targeted muscles was reduced to 75% and 25% of the baseline in the mild and severe degeneration models, respectively. Comparison

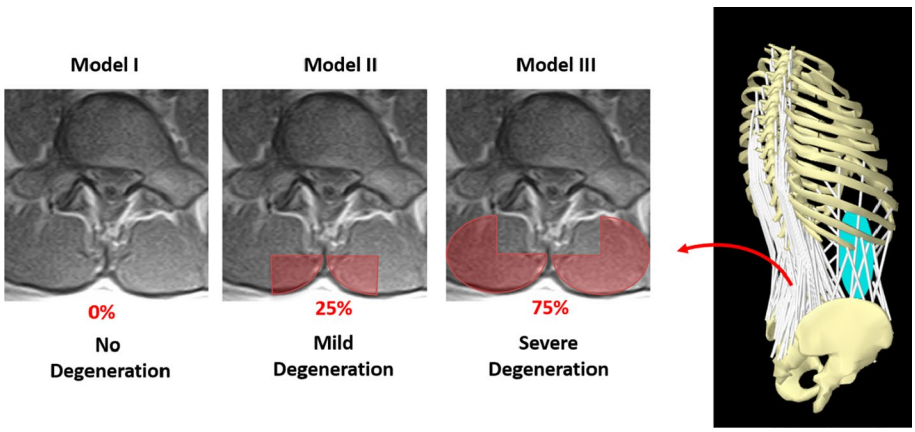

Fig. 2 Musculoskeletal models used. Note that muscle cross-sectional areas were the same between the models and only their biomechanical properties were changed. Model I (baseline) had no muscle degeneration as opposed to the other two models in which 25% (model II, representing mild degeneration) and 75% (model III, representing severe degeneration) of the healthy contractile tissue was replaced by degenerated (stiffer) muscle fiber bundles in each of multifidus, longissimus, and iliocostalis. The MRI image is adapted from [43] through open access provided by BMC medicine

of the L4–L5 IDP between the three models was made for three sarcomere length conditions: (1) in-situ sarcomere length and slack sarcomere length baseline values; (2) sarcomere length parameters were 0.5 microns longer; (3) or shorter than baseline.

Results

All biopsies were collected as planned; the only exceptions were Type B2 biopsies for patient 1 (which were used as Type B1 biopsies due to their small size) and longissimus biopsies, Type A and B, for patient 3 (as the surgical exposure was only limited to multifidus).

In-situ sarcomere length

In total, 34 type A biopsies were collected. Three biopsies consisted of non-muscle tissue although they were collected by the surgeon from the same anatomical locations as the other biopsies. From the remaining 31 biopsies, the average in-situ sarcomere length for each patient ranged between 1.94 µm to 3.39 µm for multifidus and 1.99 µm to 3.11 µm for longissimus (Fig. 3). Typically, within each individual there were differences in the in-situ sarcomere lengths between the convex and concave sides. With the large variability within each group, no clear differences between the three patient groups were observed, but clearly, many of the in-situ sarcomere lengths exceed literature values for non-deformity degenerative spine patients [25] (Fig. 3).

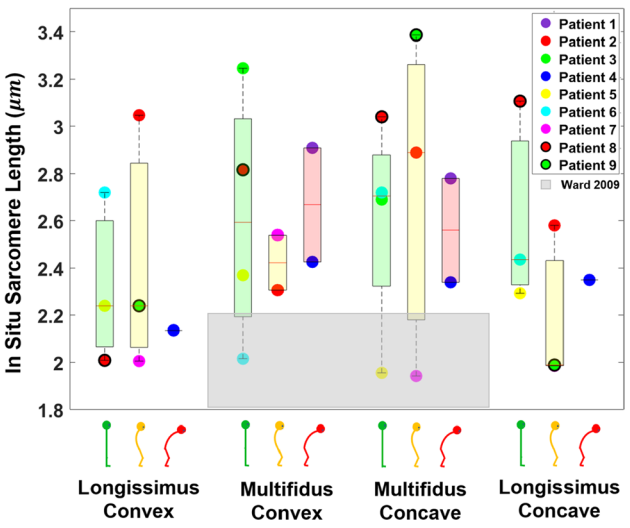

Fig. 3 In-situ sarcomere length represented by boxplots for each patient group. The red lines denote the medians, the heights of the boxes indicate the interquartile ranges and each dot is the average of three measurements for each biopsy (the three measurements were quite consistent for almost all biopsies). Green, yellow, and red icons along the *x*-axis represent patient groups I, II, and III, respectively. The gray box represents the mean ± standard error of the in-situ sarcomere length reported in the single study that has measured it in multifidus only [25]

Passive elastic modulus and slack sarcomere length

In total, 87 fibers and 171 fiber bundles were passively tested. The single fiber elastic modulus ranged between 2 to 115 kPa for multifidus and 5 kPa to 94 kPa for longissimus (Fig. 4). The median values are consistent with literature values for non-deformity spinal degenerative patients, but with noticeably wider variability [22] (Fig. 4).

The fiber bundle elastic modulus ranged between 6 and 2426 kPa for multifidus and 3 kPa to 2375 kPa for longissimus (Fig. 5). Seventeen of 92 tested multifidus bundles (18%) and 20 of 79 longissimus bundles (25%) exhibited elastic moduli larger than 120 kPa (i.e. approximate threshold for outliers in non-deformity spinal degenerative patients, Ward et al. [22]). No statistical comparison was made, as outlined previously.

Slack sarcomere lengths exhibited a large range (1.8–2.8 µm) for both fibers and fiber bundles (Fig. 6). With the large variability within each group, no clear differences between the three patient groups were observed, nor was statistical analysis performed as outlined previously. However, it is clear that many of the slack sarcomere lengths varied widely from literature values [22].

Specific force

Eight of 34 (24%) collected biopsies did not exhibit any contractile properties. From the remaining biopsies, a total of 86 fibers underwent active testing for specific force. 84 were type 1 fibers and 2 were type 2a fibres; therefore, only type 1 fibres are reported here. Specific force ranged between 22 to 233 kPa for multifidus and 28 kPa to 180 kPa for longissimus (Fig. 7). The median values are generally below average age-matched literature norms for type 1 fibers from vastus lateralis, see Fig. 7.

Histopathological analysis

Twenty-eight biopsies were successfully frozen, sectioned, and stained. The histological appearance was normal for only one patient (patient 6, Fig. 8a–c). The amount of fibrofatty tissue varied across biopsies (Fig. 8d–h), in some cases with severe atrophy and fibrosis (patient 4, Fig. 8d–e). A variety of case-specific fiber abnormalities were observed (Table 2) including core/target and cox-negative fibers (Patient 2, Fig. 9a–d), cores and rods (patient 3, Fig. 9e–g), mitochondrial accumulations (patient 5, Fig. 9h–j), and moth-eaten fibers and pin-prick fibers (patient 7, Fig. 9k–m). In general, the magnitude

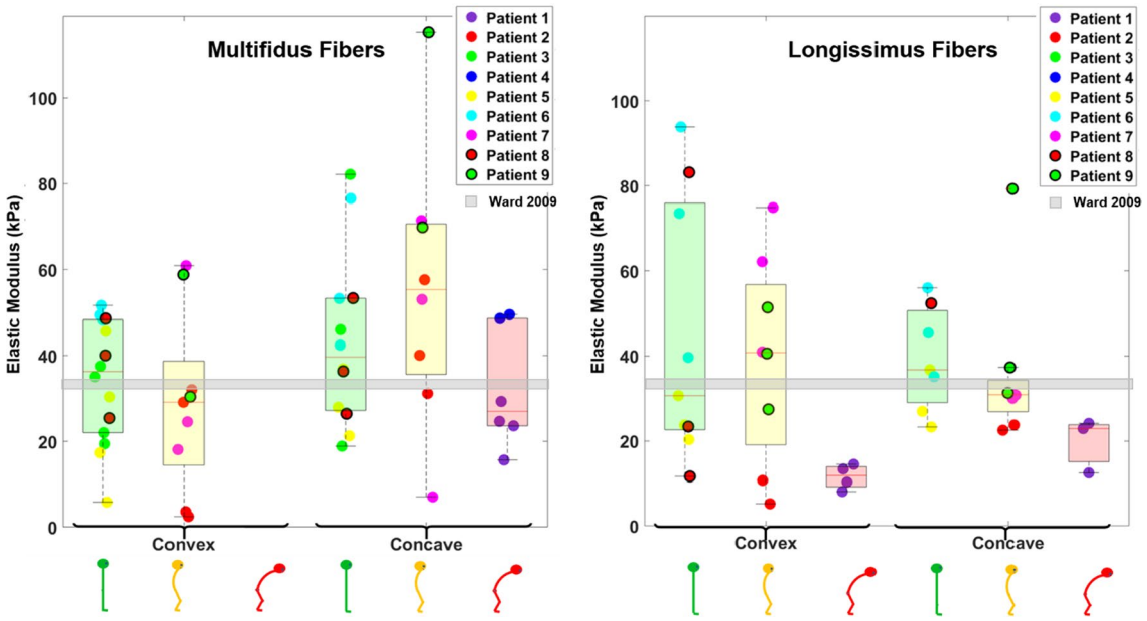

Fig. 4 Passive elastic modulus of single fibers represented by boxplots for each patient group. The red lines denote the medians, the heights of the boxes indicate the interquartile ranges and each dot represents the elastic modulus value for a tested fiber bundle. Green, yellow, and red icons along the *x*-axis represent patient groups I, II, and III, respectively. The gray box represents the mean ± standard error of the elastic modulus reported in the single study that measured this from live human biopsies [22]

of abnormality was more severe in patients of group II and III (Table 3).

Musculoskeletal modeling

All the biomechanical muscle properties investigated in this study impacted spinal loading. In general, greater magnitudes of muscle degeneration (i.e. higher elastic modulus and lower specific force) were associated with higher intradiscal pressures (IDP), with a clear influence of in-situ and slack sarcomere lengths, and posture (Fig. 10). The elevated IDP due to muscle degeneration was more evident for shorter slack and longer in-situ sarcomere lengths. For example, in standing the IDP increased from 0.38 MPa in the baseline model to 0.53 MPa (39% increase) in the model with severe muscle degeneration. When slack sarcomere length was set to be 0.5 µm shorter than baseline (i.e. 2.3 compared to 2.8 µm), the L4–L5 IDP in standing reached 1.48 MPa (289% increase) in the model with severe degeneration. The same trends, but amplified, were evident in the flexed posture due to the development of higher passive forces, such that the IDP reached beyond 500% of the baseline value.

Discussion

Decreased spinal extensor strength is a well-recognized risk factor for ASD and post-operative PJF, but it remains unknown what role intrinsic muscle properties play in this condition. One reason for this lack of understanding is the challenge associated with acquiring fresh human muscle biopsies, which are necessary for measurement of muscle properties including passive stiffness (elastic modulus), slack sarcomere length, in-situ sarcomere length, and specific force. This study aimed to address these challenges by obtaining biopsies from ASD patients and evaluating them biomechanically and histopathologically. Our key findings included observation of substantially stiff fiber bundles in the paraspinal muscles of these patients, which links well with the observed fibrosis in the muscle, as well as compromised paraspinal muscle contractile function. Although patient recruitment halted due to COVID-19, limiting the sample size, these observations provide considerable insight into the paraspinal muscles of ASD patients.

Several biomechanical properties of the paraspinal muscle in ASD patients were observed to be different from literature values for non-deformity spine degenerative patients;

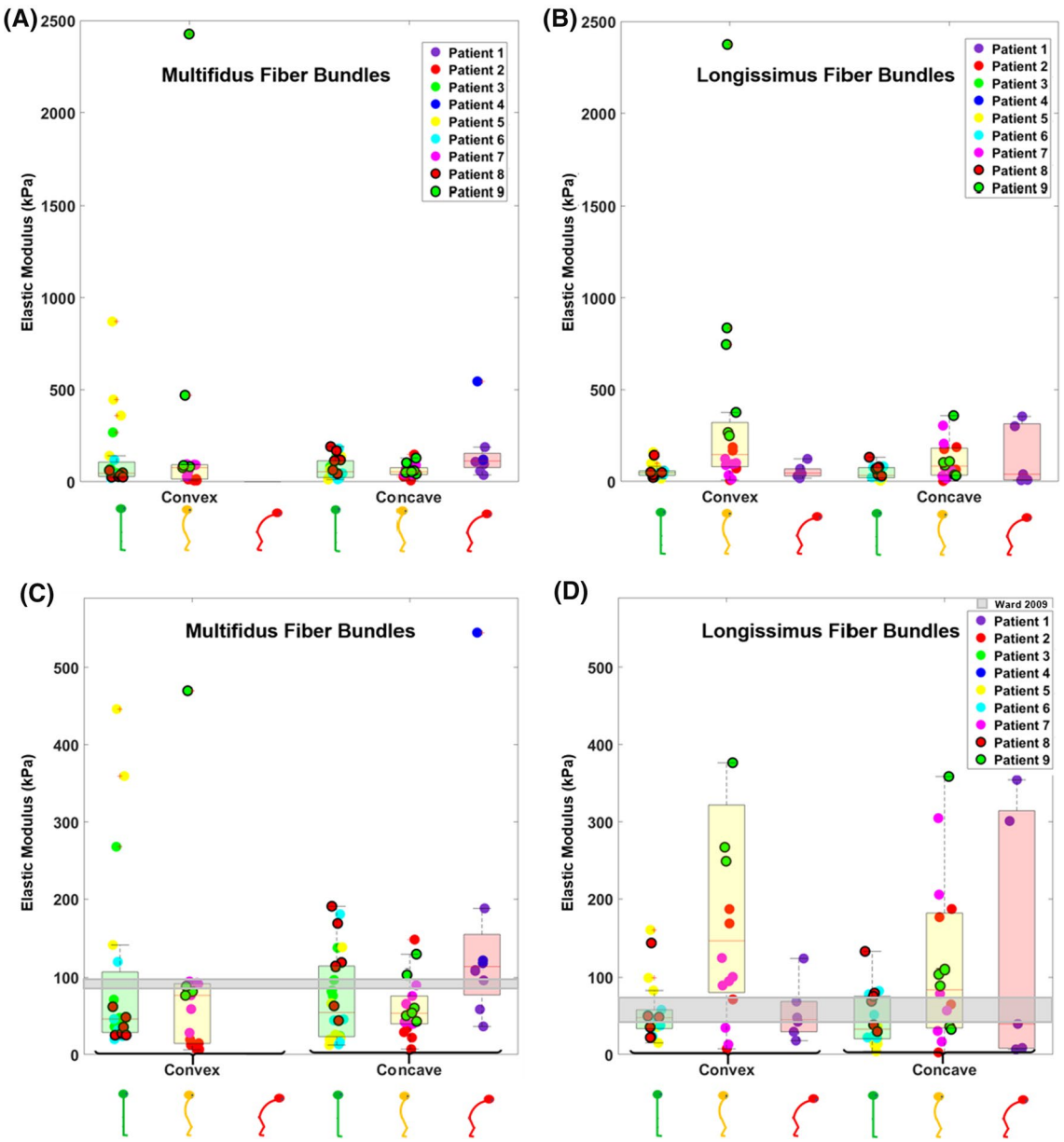

Fig. 5 Passive elastic modulus of fiber bundles represented by box-plots for each patient group. **a**, and **b** are the same plots as **c** and **d** but with a larger scale on the *y*-axis to encompass all data points. The red lines denote the medians, the heights of the boxes indicate the inter-quartile ranges and each dot represents the elastic modulus value for a tested fiber bundle. Green, yellow, and red icons along the *x*-axis represent patient groups I, II, and III, respectively. The gray box represents the mean ± standard error of the elastic modulus reported in the single study that measured this from live human biopsies [22]

modeling these abnormal properties identified significant biomechanical consequences. Specifically, ~ 20% of the muscle fiber bundles tested had very high passive stiffness (Fig. 5), and the muscle fiber specific force was generally low (Fig. 7), with notably ~ 24% of the muscle samples exhibiting no contractile function. The in-situ sarcomere lengths were greater than the average literature values (Fig. 3), and the slack sarcomere lengths exhibited high variability, with means near literature values (Fig. 6). Certain combinations of these properties in a patient will increase the potential for excessively high spinal compressive forces (Fig. 10), which could exacerbate the deformity or be the nexus for post-surgical complications such as PJF.

Muscle passive elastic modulus in this study was evaluated at both the single fiber and fiber bundle levels. The median values of our study are in good agreement with the literature for single fibers [22]. We observed greater elastic moduli for fiber bundles compared to single fibres, which is

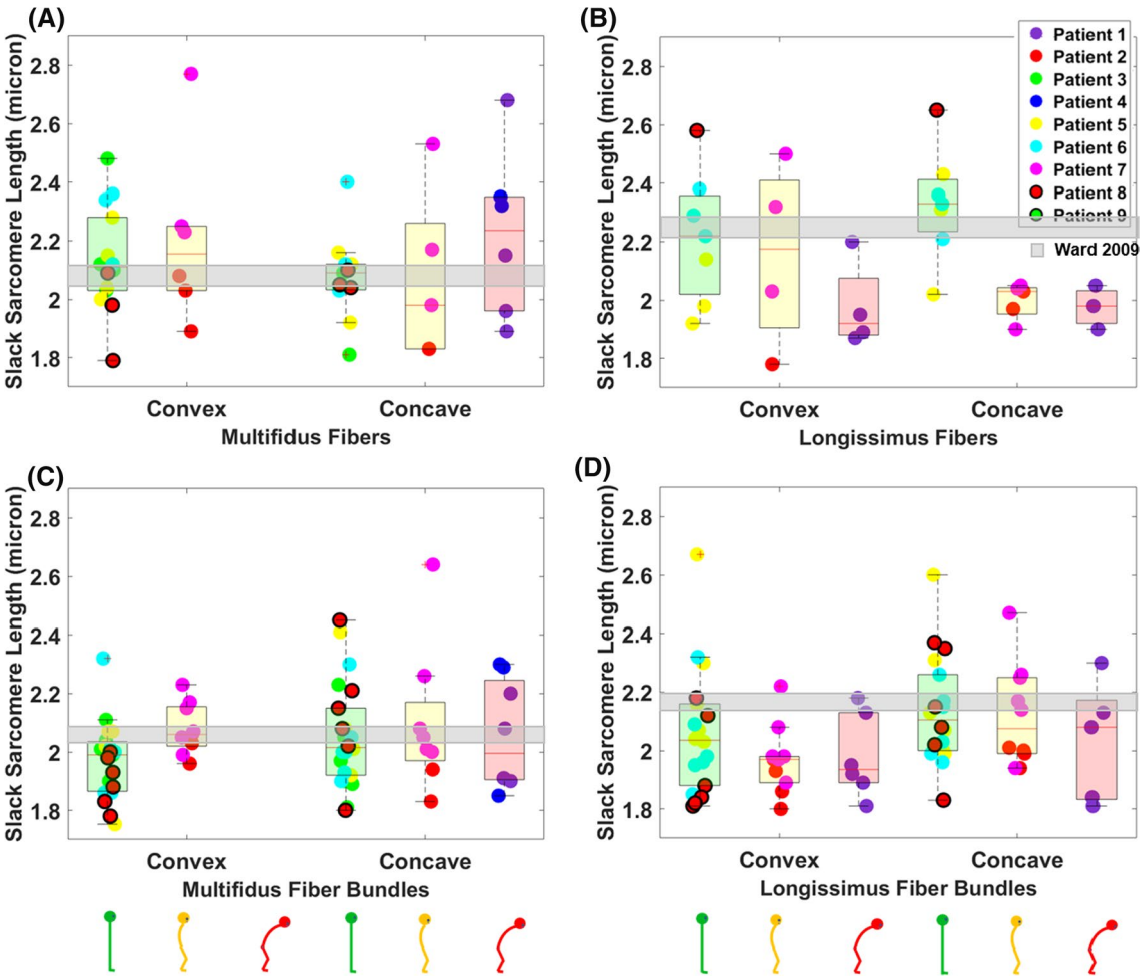

Fig. 6 Slack sarcomere length represented by boxplots for each patient group. The red lines denote the medians, the heights of the boxes indicate the interquartile ranges and each dot represents slack sarcomere length value for a tested fiber. Green, yellow, and red icons along the *x*-axis represent patient groups I, II, and III, respectively. The gray box represents the mean ± standard error of the slack sarcomere lengths reported in the single study that measured this from live human biopsies [22]

also consistent with the literature, due to the stiffening role of the extracellular matrix [23, 34–37]. The notable observation in our data was that 37 of 171 bundles (22%) exhibited very large elastic moduli for both multifidus and longissimus muscle groups. The elastic moduli for these bundles, which were more prevalent for group II patients, were mostly between 200 to 1000 kPa but even reached above ~ 2000 kPa in two cases. This very stiff passive behavior at the bundle level is likely due to fibrosis [38] and may have pathologic roots, which should be explored further.

This is the first study to investigate and report on the active mechanical properties of human spine muscles. Muscle fiber specific force represents the inherent ability of the fiber to generate contractile force. Our observations provide support for an association between spine pathology and impaired contractile function as the mean specific force values reported here are below reported literature values for type I muscle fibers from the vastus lateralis of older individuals [26–29] (males and females combined; age range: 65–85 years; see Fig. 7). Further, 24% of biopsies had no contractile ability, suggesting severe dysfunction. While this study provides the first report on the active contractile function of human spine muscles, any comparison with data from other muscles (e.g. vastus lateralis) should be made with caution, and efforts should be focused on collecting normative contractile data from healthy human spine muscles.

The in-situ and slack sarcomere lengths measured in this study revealed a larger range for human paraspinal muscles than observed previously by Ward et al. for non-deformity degenerative spine patients [22, 25]. Such large variation can result in a substantially different behavior and affect the amount of active and passive force a muscle produces. Since passive force increases in a non-linear manner at lengths beyond slack, slack sarcomere length and spine posture

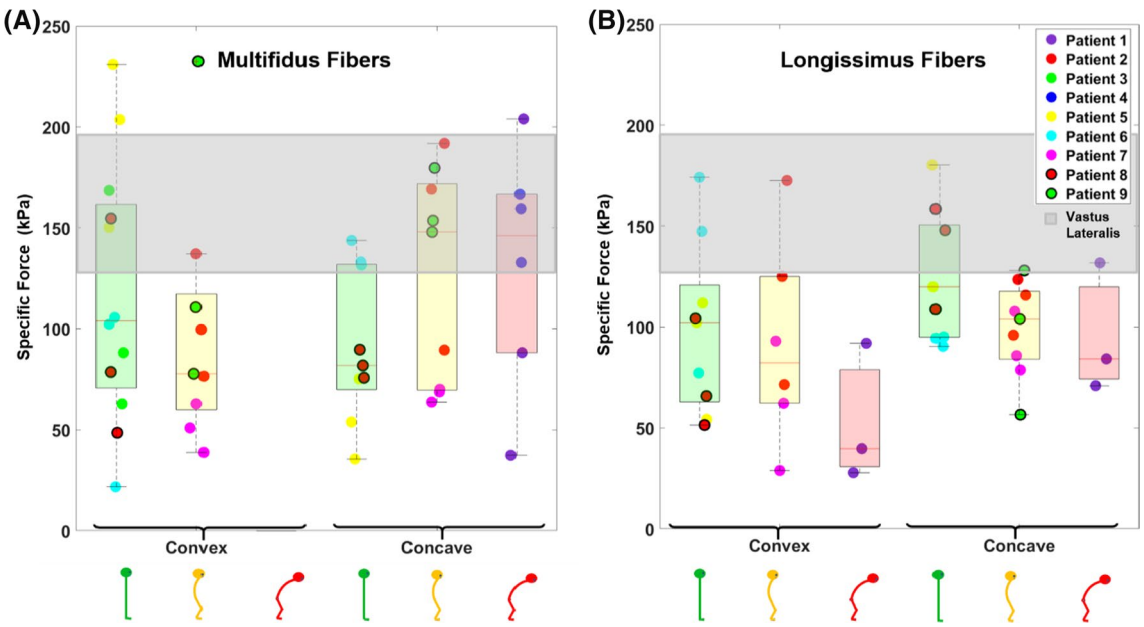

Fig. 7 Specific force values of type 1 single muscle fibers from the multifidus and longissimus represented by box and whisker plots for each patient. The red lines represent the median, while the height of the boxes indicate the 25th to 75th percentiles, the whiskers represent the minimum and maximum values, and each dot represents the specific force value for a single muscle fiber. Green, yellow, and red icons along the *x*-axis represent patient groups I, II, and III, respectively. The gray box represents the mean ± standard deviation of the average specific forces reported for elderly human vastus lateralis (65–85 years old) in the literature [26–29]

interact to significantly influence passive force generation. For shorter slack sarcomere lengths, larger passive forces will develop, especially when the body goes into a flexed posture, where the paraspinal extensor muscles experience greater elongation. Investigating the influence of these sarcomere length parameters is complex, thereby necessitating the use of a musculoskeletal model in the current study.

Our biomechanical modelling revealed that there is a clear interplay between these various muscle parameters as it relates to spine loading, and that posture plays an important role. For example, in flexed postures, spinal loads can increase by as much as five times baseline for patients with high muscle stiffness, short slack sarcomere lengths, and long in-situ sarcomere lengths. Given the wide range of data values in these nine patients, scenarios such as this appear likely.

The histopathological analysis of the biopsies identified a variety of abnormalities at both the cellular and tissue levels. Biopsies from only 1 of 9 patients appeared normal. At the tissue level, fibrosis was evident in some cases and was greatest for patient 4. At the cellular level, moth-eaten fibers, pinprick fibers, core and targets and cox negative fibers were often identified. The interpretation of different fiber pathologies in paraspinal muscle is less certain than in more frequently biopsied appendicular muscles, because of little clinical experience with biopsies from these sites. As a consequence, a cautious approach appears justified. The variety of structural and mitochondrial abnormalities observed in our study is suggestive of diverse and complex mechanisms of potential functional impairment. Interestingly, on average the severity of the abnormalities was qualitatively highest for paraspinal muscles of group III patients, moderate for group II and were somewhat mild to moderate in group I. However, this is a preliminary analysis and more patients are required to identify patterns or make meaningful comparisons between the study groups.

This study is the first to document such degenerative changes for human longissimus muscles, and the first to report on multifidus and longissimus in patients with ASD. Two recent studies on multifidus histopathology noted similar extracellular and intracellular observations to the present study [39, 40]. Padwal et al. [39] histologically examined superficial and deep regions of multifidus in 16 patients with lumbar spine pathologies (12 stenosis, 2 spondylolisthesis, and 2 disc herniation) and found an elevated amount of muscle degeneration/regeneration markers compared to normal muscles in the literature. The overall multifidus composition in their study was 11% ± 9% fat, 49% ± 16% muscle, and 26% ± 12% collagen with no statistically significant difference between the deep and superficial regions of multifidus. Shahidi et al. [40] also examined the multifidus of 10 acute and 22 chronic patients with degenerative lumbar spine pathologies and reported regional degeneration and punctate necrosis within muscle fibers with no difference between the

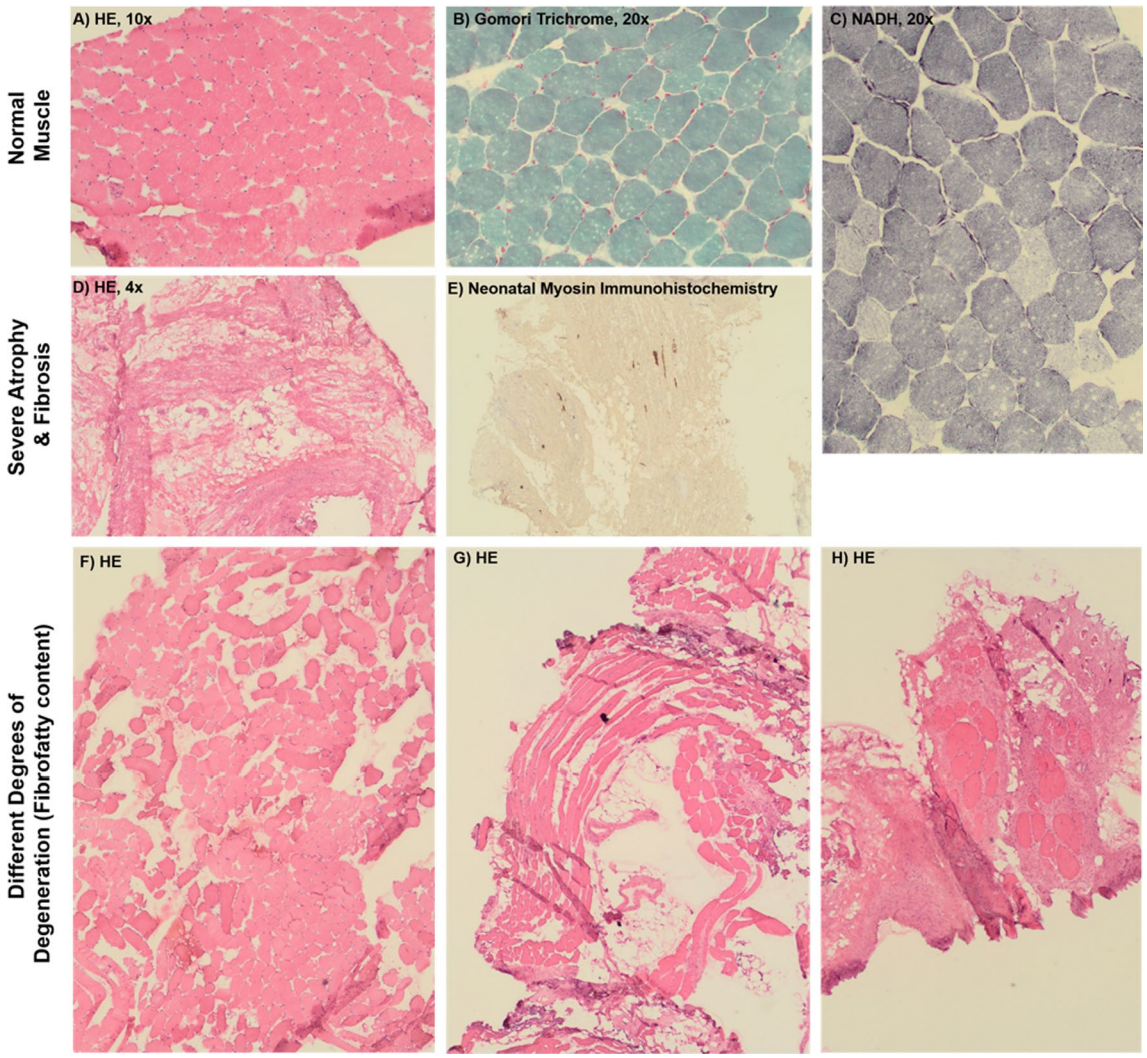

Fig. 8 Illustration of variable degrees of fibro-fatty replacement in paraspinal muscle biopsies from ASD patients. **a**–**c** Fairly normal biopsy with regular internal architecture of muscle fibers. **d**–**e**) Severe fibrosis. Scarce remaining muscle fibers are only identified on immunohistochemical stain for neonatal myosin. **f**–**h** Variable degrees of fibro-fatty replacement on H&E stained sections with scattered fat cells in **f**, increasing and regional fatty replacement and fibrosis in **g**, and significant fibrosis with increased size variability of remaining fibers in **h**

Table 2 Main abnormality types identified for each patient through histopathological evaluation

Group	Patient	Longissimus convex	Multifidus convex	Multifidus concave	Longissimus concave
I	P3	N/A[a]	Rods Cox-negative Core like	Rods Core like	N/A
	P5	Atrophic fibers	Mitochondrial	Mitochondrial	Atrophic fibers
	P6	None	None	None	N/A
	P8	Lobulated	Moth-eaten	Moth-eaten	Lobulated
II	P2	Cores	Cores, Cox-negative	Cores, Cox-negative	Cores
	P7	Moth-eaten Pinprick	Moth-eaten Pinprick	Moth-eaten Pinprick	Moth-eaten Pinprick
	P9	No Muscle	Rods and Cores	Irregular staining	Freezing Artifact
III	P4	Fibrotic Replacement	Fibrotic Replacement	Fibrotic Replacement	Fibrotic Replacement

[a]N/A refers to the cases where for minimal exposure only multifidus biopsies were collected or the biopsy size was not sufficient for histology processing

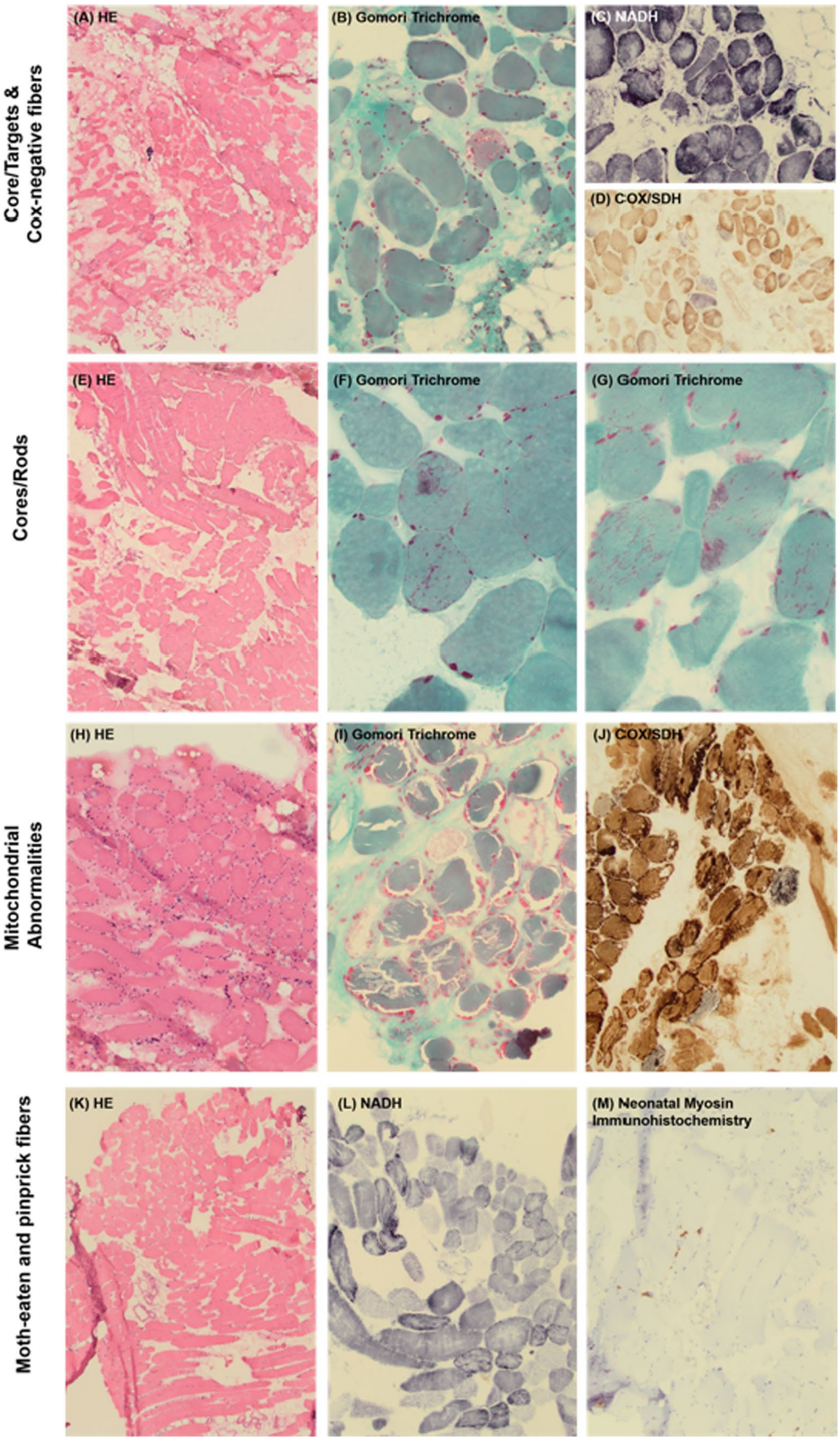
Core/Targets & Cox-negative fibers
(A) HE
(B) Gomori Trichrome
(C) NADH
(D) COX/SDH
Cores/Rods
(E) HE
(F) Gomori Trichrome
(G) Gomori Trichrome
Mitochondrial Abnormalities
(H) HE
(I) Gomori Trichrome
(J) COX/SDH
Moth-eaten and pinprick fibers
(K) HE
(L) NADH
(M) Neonatal Myosin Immunohistochemistry

◂**Fig. 9** Illustration of muscle fiber abnormalities found in paraspinal muscle biopsies from ASD patients. **a–d** Biopsy showing core/target fibers on the NADH stain (**c**), mitochondrial abnormalities on **b**, and Cox-negative fibers on the combined COX/SDH stain **d**. **e–g**) Biopsy showed rod like structures on the Gomori Trichrome stain, central deposits consistent with cores, and cytoplasmic bodies. **h–j** Biopsy showed significant mitochondrial abnormalities with subsarcolemmal accumulation apparent on the trichrome stain and Cox-negative fibers on the COX/SDH stain. **k–m**) Milder fiber pathology exemplified by moth-eaten changes to the internal architecture on the NADH stain and presence of highly atrophic, neonatal-myosin-positive fibers ('pin-prick fibers') on immunohistochemistry

acute and chronic patients. The regional differences were mostly characterized by cellular infiltration, cytoplasmic disruption, and membrane disruption.

There were several limitations to this study that should be considered when interpreting the results. First, due to patient recruitment being halted by COVID-19, the number of patients (four in group I, three in group II and two in group III) was too small to make comparisons between the patient groups. Second, as a non-invasive collection of biopsies from a healthy population was not feasible or ethically possible, there was no true healthy control group. Further, although a previous history of spine surgery or coronal plane deformity were initially set as exclusion criteria, these criteria were removed to increase enrollment (patients 1 & 9). This may have introduced confounding variability, particularly with respect to the impact of previous surgery on muscle properties. Third, given the relatively small size and poor quality (of some) of the biopsy muscle tissue, extracting three fibers or six fiber bundles for the passive and active biomechanical tests was not possible for all biopsies. This led to uneven sample sizes between the biopsies and the patients.

We conclude that the loss of paraspinal muscle strength in ASD is due to a variety of cellular and extracellular abnormalities observed that suggest a diverse and complex array of mechanisms underlying the potential functional impairment. The large variations observed for in situ sarcomere length, slack sarcomere length, and elastic modulus, combined with reduced contractile function, can lead to high spinal compression loading.

Appendix 1: Rule of mixtures for calculating elastic modulus of degenerated muscles

For musculoskeletal modeling, the passive elastic modulus at the whole muscle level is desired. Paraspinal muscle passive elastic modulus at the whole muscle level has not been reported to date for any species. However, this property for animal lower extremity muscles has been measured in the range of 1 to 10 MPa (at 30% strain) as opposed to the elastic modulus of muscle fiber bundles which was at the order of ~ 50 kPa [41]. The nonlinear passive elastic modulus curve in our musculoskeletal model was adopted from the study by Millard et al. [33] and the tangent modulus at 30% strain was 1 MPa for all muscles in our musculoskeletal model. As collagen seems to be a strong predictor of muscle passive function [41] and assuming a difference of ~ 10% in collagen content between the whole muscle and normal muscle fiber bundles [41], we calculated the elastic modulus of whole muscle connective tissue using the rule of mixtures for composites as:

$$E_{\text{WholeMuscle}} = f_{\text{Bundles}} E_{\text{Bundles}} + \left(1 - f_{\text{Bundles}}\right) E_{\text{Con.Tissue}}$$

where $E_{\text{WholeMuscle}}$, E_{Bundles}, and $E_{\text{Con.Tissue}}$ are the elastic moduli of the whole muscle, the muscle fiber bundles, and the connective tissue, respectively; and f_{Bundles} denotes the percentage of the muscle fiber bundles within the whole muscle (excluding any connective tissue beyond the muscle fiber bundles such as perimysium, epimysium, etc.). Therefore, we have:

$$1\text{MPa} = 0.9 \times 50 + (1 - 0.9) E_{\text{Con.Tissue}}$$

through which we obtain:

$$E_{\text{Con.Tissue}} = 9550\,\text{kPa}$$

We assumed the elastic modulus and percentage of connective tissue beyond muscle fiber bundles remain constant. However, the elastic modulus of the muscle fiber bundles would be different for different magnitudes of muscle degeneration and can be obtained through the following rule of mixtures:

$$E_{\text{Bundles}} = f_{\text{NormalBundles}} E_{\text{NormalBundles}} + \left(1 - f_{\text{NormalBundles}}\right) E_{\text{StiffBundles}}$$

where E_{Bundles} is the equivalent elastic modulus of the muscle fiber bundles, $E_{\text{NormalBundles}}$ is the elastic modulus of normal muscle fiber bundles (i.e. 50 kPa), and $E_{\text{StiffBundles}}$ is elastic modulus of stiff muscle fiber bundles (i.e. ~ 2000 kPa in this study); and $f_{\text{NormalBundles}}$ denotes the percentage of the muscle tissue that remains healthy with no degeneration. Therefore, for the case of mild degeneration where 25% of the normal muscle fiber bundles are replaced by stiff muscle fiber bundles, the equivalent elastic modulus would be:

$$E_{\text{Bundles}}^{25\%\text{degeneration}} = 0.75 \times 50 + (1 - 0.75) \times 2000 = 538\,\text{kPa}$$

This means the elastic modulus at the whole muscle level would be:

$$\begin{aligned} E_{\text{WholeMuscle}}^{25\%\text{degeneration}} &= f_{\text{Bundles}} E_{\text{Bundles}} + \left(1 - f_{\text{Bundles}}\right) E_{\text{Con.Tissue}} \\ &= 0.9 \times 538 + (1 - 0.9) \times 9550 = 1439\,\text{kPa} \end{aligned}$$

which implies the targeted muscles in the model with mild degeneration would be 1.44 times stiffer than the baseline

Table 3 Magnitude of histological abnormality for each patient

Group	Patient	Longissimus Convex	Multifidus Convex	Multifidus Concave	Longissimus Concave
I	P3	N/A	Moderate	Moderate	N/A
	P5	Mild	Moderate	Moderate	Mild
	P6	Normal	Normal	Normal	N/A
	P8	Moderate	Minor	Minor	Moderate
II	P2	Moderate	Severe	Severe	Moderate
	P7	Minor	Minor	Minor	Minor
	P9	No Muscle	Moderate	Minor	Freezing Artifact
III	P4	Severe	Severe	Severe	Severe

*N/A refers to the cases where for minimal exposure only multifidus biopsies were collected or the biopsy size was not sufficient for histology processing.

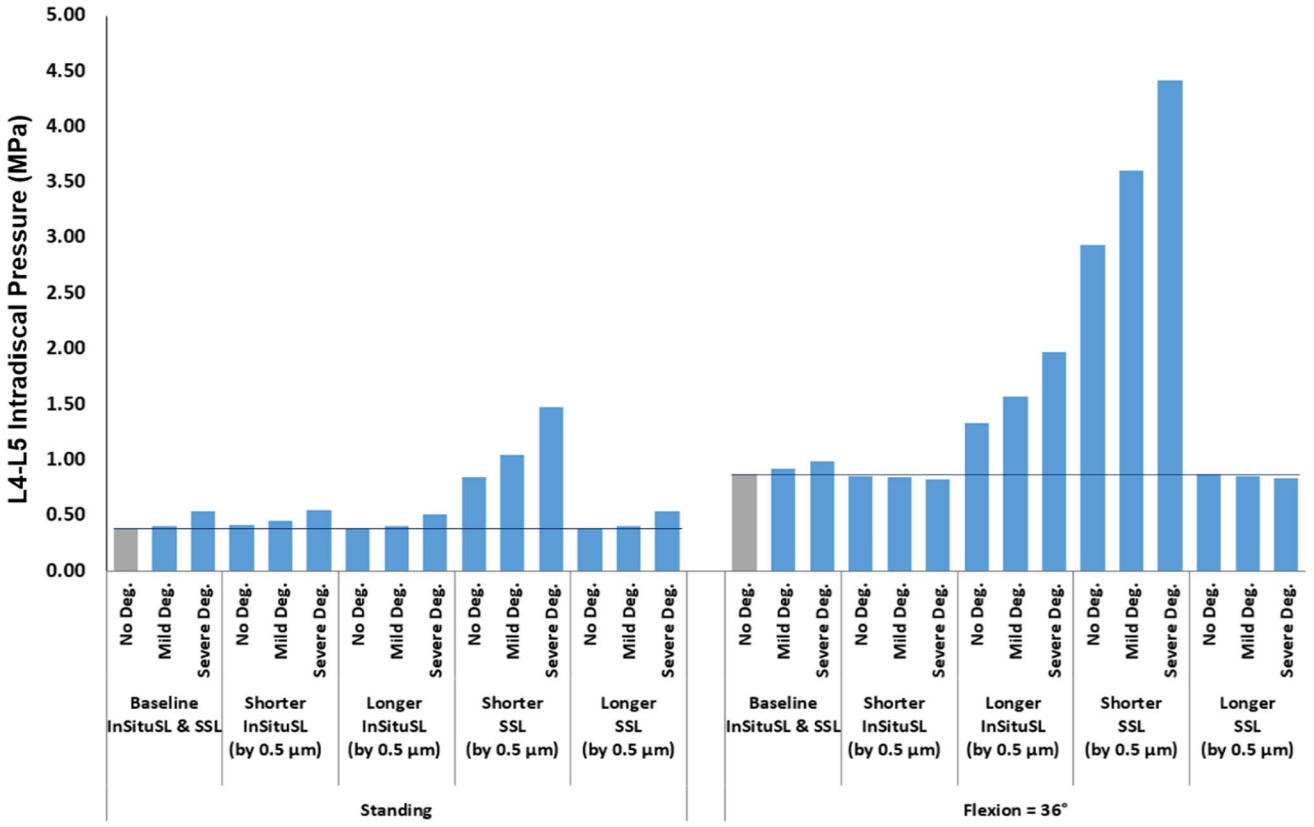

Fig. 10 Predicted L4–L5 intradiscal pressure by the musculoskeletal model for three different conditions: no muscle degeneration, mild muscle degeneration, and severe muscle degeneration. In-situ sarcomere lengths and slack sarcomere lengths were also varied, as was posture (upright standing compared to standing with 36° spine flexion)

model. Similarly, the elastic modulus of the targeted muscles in the model with 75% degeneration was calculated as 2317 kPa (i.e. 2.32 times stiffer than the baseline model).

Funding This study received support and funding from Medtronic Canada and the Natural Sciences and Engineering Research Council of Canada.

Availability of data and material All data are available upon request.

Code availability The software package used in this study is open-source and the codes used for this study are available at GitLab.

Declarations

Conflict of interest The authors declare no conflicts of interest.

Ethics approval The human study was approved by Vancouver Coastal Health Research Institute (VCHRI) and the Clinical Research Ethics Board (CREB) of the University of British Columbia, Vancouver, Canada.

Consent to participate Informed consent was obtained from all patients and all methods including biopsy collection were carried out in accordance with relevant guidelines and regulations.

Consent for publication All the authors consented to publication of this manuscript.

References

1. Kado DM, Prenovost K, Crandall C (2007) Narrative review: hyperkyphosis in older persons. Ann Intern Med 147(5):330–338
2. Ames CP, Scheer JK, Lafage V, Smith JS, Bess S, Berven SH, Mundis GM, Sethi RK, Deinlein DA, Coe JD, Hey LA, Daubs MD (2016) Adult spinal deformity: epidemiology, health impact, evaluation, and management. Spine Deform 4(4):310–322
3. Lafage R, Beyer G, Schwab F, Klineberg E, Burton D, Bess S, Kim HJ, Smith J, Ames C, Hostin R, Khalife M, Shaffrey C, Mundis G, Lafage V (2020) Risk factor analysis for proximal junctional kyphosis after adult spinal deformity surgery: a new simple scoring system to identify high-risk patients. Glob Spine J 10(7):863–870
4. Katzman WB, Wanek L, Shepherd JA, Sellmeyer DE (2010) Age-Related hyperkyphosis: its causes, consequences, and management. J Orthop Sport Phys Ther 40(6):352–360
5. Roghani T, Zavieh MK, Manshadi FD, King N, Katzman W (2017) Age-related hyperkyphosis: update of its potential causes and clinical impacts—narrative review. Aging Clin Exp Res 29(4):567–577
6. Sinaki M, Itoi E, Rogers JW, Bergstralh EJ, Wahner HW (1996) Correlation of back extensor strength with thoracic kyphosis and lumbar lordosis in estrogen-deficient women. Am J Phys Med Rehabil 75(5):370–374
7. Sinaki M, Brey RH, Hughes CA, Larson DR, Kaufman KR (2005) Balance disorder and increased risk of falls in osteoporosis and kyphosis: significance of kyphotic posture and muscle strength. Osteoporos Int 16(8):1004–1010
8. Mika A, Unnithan VB, Mika P (2005) Differences in thoracic kyphosis and in back muscle strength in women with bone loss due to osteoporosis. Spine 30(2):241–246
9. Granito RN, Aveiro MC, Renno ACM, Oishi J, Driusso P (2012) Comparison of thoracic kyphosis degree, trunk muscle strength and joint position sense among healthy and osteoporotic elderly women: a cross-sectional preliminary study. Arch Gerontol Geriatr 54(2):e199–e202
10. Weale R, Weale M (2012) The Dowager's hump: an early start? Gerontology 58(3):212–215
11. Beschloss A, Dicindio C, Lombardi J, Varthi A, Ozturk A, Lehman R, Lenke L, Saifi C (2021) Marked increase in spinal deformity surgery throughout the United States. Spine 46(20):1402–1408
12. Haldeman PB, Swan AR, Ward SR, Osorio J, Shahidi B (2021) Letter to the Editor Re: 'State of the art: proximal junctional kyphosis—diagnosis, management and prevention.' Spine Deform 1–10
13. Pennington Z, Cottrill E, Ahmed AK, Passias P, Protopsaltis T, Neuman B, Kebaish KM, Ehresman J, Westbroek EM, Goodwin ML, Sciubba DM (2019) Paraspinal muscle size as an independent risk factor for proximal junctional kyphosis in patients undergoing thoracolumbar fusion. J Neurosurg Spine 31(3):380–388
14. Kang CH, Shin MJ, Kim SM, Lee SH, Lee CS (2007) MRI of paraspinal muscles in lumbar degenerative kyphosis patients and control patients with chronic low back pain. Clin Radiol 62(5):479–486
15. Hyun SJ, Kim YJ, Rhim SC (2016) Patients with proximal junctional kyphosis after stopping at thoracolumbar junction have lower muscularity, fatty degeneration at the thoracolumbar area. Spine J 16(9):1095–1101
16. Park KH, Oh JS, An DH, Yoo WG, Kim JM, Kim TH, Kang MH (2015) Difference in selective muscle activity of thoracic erector spinae during prone trunk extension exercise in subjects with slouched thoracic posture. PM R 7(5):479–484
17. Lieber RL, Runesson E, Einarsson F, Fridén J (2003) Inferior mechanical properties of spastic muscle bundles due to hypertrophic but compromised extracellular matrix material. Muscle Nerve 28(4):464–471
18. Fridén J, Lieber RL (2003) Spastic muscle cells are shorter and stiffer than normal cells. Muscle Nerve 27(2):157–164
19. Mathewson MA, Ward SR, Chambers HG, Lieber RL (2015) High resolution muscle measurements provide insights into equinus contractures in patients with cerebral palsy. J Orthop Res 33(1):33–39
20. Gumucio JP, Sugg KB, Enselman ERS, Konja AC, Eckhardt LR, Bedi A, Mendias CL (2018) Anterior cruciate ligament tear induces a sustained loss of muscle fiber force production. Muscle Nerve 58(1):145–148
21. Mendias CL, Roche SM, Harning JA, Davis ME, Lynch EB, Sibilsky Enselman ER, Jacobson JA, Claflin DR, Calve S, Bedi A (2015) Reduced muscle fiber force production and disrupted myofibril architecture in patients with chronic rotator cuff tears. J Shoulder Elb Surg 24(1):111–119
22. Ward SR, Tomiya A, Regev GJ, Thacker BE, Benzl RC, Kim CW, Lieber RL (2009) Passive mechanical properties of the lumbar multifidus muscle support its role as a stabilizer. J Biomech 42(10):1384–1389
23. Yamamoto S, Malakoutian M, Theret M, Street J, Rossi F, Brown SHM, Saito M, Oxland TR (2021) The effect of posterior lumbar spinal surgery on biomechanical properties of rat paraspinal muscles 13 weeks after surgery. Spine 46(21):E1125–E1135
24. Noonan AM, Séguin CA, Brown SHM (2021) Paraspinal muscle contractile function is impaired in the ENT1-deficient mouse model of progressive spine pathology. Spine 46(13):E710–E718
25. Ward SR, Kim CW, Eng CM, Gottschalk LJ IV, Tomiya A, Garfin SR, Lieber RL (2009) Architectural analysis and intraoperative measurements demonstrate the unique design of the multifidus muscle for lumbar spine stability. J Bone Jt Surg - Ser A 91(1):176–185
26. Reid KF, Doros G, Clark DJ, Patten C, Carabello RJ, Cloutier GJ, Phillips EM, Krivickas LS, Frontera WR, Fielding RA (2012) Muscle power failure in mobility-limited older adults: preserved single wber function despite lower whole muscle size, quality and rate of neuromuscular activation. Eur J Appl Physiol 112(6):2289–2301
27. Slivka D, Raue U, Hollon C, Minchev K, Trappe S (2008) Single muscle fiber adaptations to resistance training in old (>80 yr) men: evidence for limited skeletal muscle plasticity. Am J Physiol Regul Integr Comp Physiol 295(1):R273–R280
28. Krivickas LS, Fielding RA, Murray A, Callahan D, Johansson A, Dorer DJ, Frontera WR (2006) sex differences in single muscle fiber power in older adults. Med Sci Sports Exerc 38(1):57–63
29. Trappe S, Gallagher P, Harber M, Carrithers J, Fluckey J, Trappe T (2003) Single muscle fibre contractile properties in young and old men and women. J Physiol 552(1):47–58

30. Malakoutian M (2021) Biomechanical properties of paraspinal muscles and their influence on spinal loading - an experimental and computational investigation. PhD Thesis. University of British Columbia
31. Malakoutian M, Yamamoto S, Sadaram S, Speidel J, Liu J, Street J, Brown SHM, Oxland TR (2021) The effect of vertebral level on biomechanical properties of the lumbar paraspinal muscles in a rat model. J Mech Behav Biomed Mater 118:104446
32. Malakoutian M, Sanchez CA, Brown SHM, Street J, Fels S, Oxland T (2022) Biomechanical properties of paraspinal muscles influence spinal loading—a musculoskeletal simulation study. Front Bioeng Biotechnol 10:852201
33. Millard M, Uchida T, Seth A, Delp SL (2013) Flexing computational muscle: modeling and simulation of musculotendon dynamics. J Biomech Eng 135(2):21005
34. Brown SHM, Gregory DE, Carr JA, Ward SR, Masuda K, Lieber RL (2011) ISSLS prize winner: adaptations to the multifidus muscle in response to experimentally induced intervertebral disc degeneration. Spine 36(21):1728–1736
35. Zwambag DP, Gsell KY, Brown SHM (2019) Characterization of the passive mechanical properties of spine muscles across species. J Biomech 88:173–179
36. Prado LG, Makarenko I, Andresen C, Krüger M, Opitz CA, Linke WA (2005) Isoform diversity of giant proteins in relation to passive and active contractile properties of rabbit skeletal muscles. J Gen Physiol 126(5):461–480
37. Meyer GA, Lieber RL (2011) Elucidation of extracellular matrix mechanics from muscle fibers and fiber bundles. J Biomech 44(4):771–773
38. Lieber RL, Ward SR (2013) Cellular mechanisms of tissue fibrosis. 4. Structural and functional consequences of skeletal muscle fibrosis. Am J Physiol Physiol 305(3):C241–C252
39. Padwal J, Berry DB, Hubbard JC, Zlomislic V, Allen RT, Garfin SR, Ward SR, Shahidi B (2020) Regional differences between superficial and deep lumbar multifidus in patients with chronic lumbar spine pathology. BMC Musculoskelet Disord 21(1):1–9
40. Shahidi B, Gibbons MC, Esparza M, Zlomislic V, Allen RT, Garfin SR, Ward SR (2020) Cell populations and muscle fiber morphology associated with acute and chronic muscle degeneration in lumbar spine pathology. Jor Spine 3(2):e1087
41. Ward SR, Winters TM, O'Connor SM, Lieber RL (2020) Nonlinear scaling of passive mechanical properties in fibers, bundles, fascicles and whole rabbit muscles. Front Physiol 11
42. Fujibayashi S, Neo M, Takemoto M, Ota M, Nakamura T (2010) Paraspinal-approach transforaminal lumbar interbody fusion for the treatment of lumbar foraminal stenosis. J Neurosurg Spine 13(4):500–508
43. Kjaer P, Bendix T, Sorensen JS, Korsholm L, Leboeuf-Yde C (2007) Are MRI-defined fat infiltrations in the multifidus muscles associated with low back pain? BMC Med 5(1):1–10